Review Article

The role of ligand-gated conformational changes in enzyme catalysis

Ⓘ Cátia Moreira[1], Ⓘ Ana Rita Calixto[1], Ⓘ John P. Richard[2] and Ⓘ Shina Caroline Lynn Kamerlin[1]

[1]Science for Life Laboratory, Department of Chemistry - BMC, Uppsala University, BMC Box 576, S-751 23 Uppsala, Sweden; [2]Department of Chemistry, University at Buffalo, SUNY, Buffalo, New York 14260-3000, U.S.A

Correspondence: John P. Richard (jrichard@buffalo.edu) or Shina Caroline Lynn Kamerlin (lynn.kamerlin@kemi.uu.se)

Structural and biochemical studies on diverse enzymes have highlighted the importance of ligand-gated conformational changes in enzyme catalysis, where the intrinsic binding energy of the common phosphoryl group of their substrates is used to drive energetically unfavorable conformational changes in catalytic loops, from inactive open to catalytically competent closed conformations. However, computational studies have historically been unable to capture the activating role of these conformational changes. Here, we discuss recent experimental and computational studies, which can remarkably pinpoint the role of ligand-gated conformational changes in enzyme catalysis, even when not modeling the loop dynamics explicitly. Finally, through our joint analyses of these data, we demonstrate how the synergy between theory and experiment is crucial for furthering our understanding of enzyme catalysis.

Introduction

Daniel Koshland proposed in 1958 that the specificity of aminoacyl *t*-RNA synthases for charging their cognate amino acids to *t*-RNA is obtained through the utilization of binding interactions between the synthase and the cognate α-amino acid side chain, to induce a change in protein structure that draws the enzyme catalytic groups into their active conformation [1]. This induced fit proposal predicted the existence of ligand-gated conformational changes years in advance of the first enzyme X-ray crystal structure determination for egg-white lysozyme reported in 1965 [2], or the observation of such a conformational change in a comparison to the X-ray crystal structures for free triosephosphate isomerase (TIM) and for TIM complexed to substrate dihydroxyacetone phosphate (DHAP) described in 1981 [3]. Ligand-gated conformational changes have been documented for many enzymatic reactions [4], but the original induced fit proposal was criticized for a lack of clarity in the rationale for utilization of substrate binding energy to drive thermodynamically unfavorable ligand-gated conformational changes [5,6]. We have examined the mechanism of action of three enzymes that undergo ligand-gated conformational changes: TIM [7,8], orotidine 5′-monophosphate decarboxylase (OMPDC) [9], and glycerol 3-phosphate dehydrogenase (GPDH) [10,11]. We describe in this review the mechanistic rationale for the utilization of the binding energy of the phosphoryl group of the substrate (or the phosphite dianion in the case of studies of substrate fragments) to drive these ligand-gated conformational changes, the common structural elements for the three enzyme conformational changes, as well as the results of ongoing computational studies to model the role of this conformational change in catalysis by TIM.

Ligand-gated conformational changes

TIM, OMPDC, and GPDH each undergo large ligand-gated conformational changes in catalyzing the chemically diverse set of proton transfer, decarboxylation and hydride transfer reactions shown in Figure 1A [12]. The phosphoryl group of each whole substrate for these enzymes provides a ~12 kcal·mol^{-1} stabilization of the respective transition states [10,13]. One explanation for this
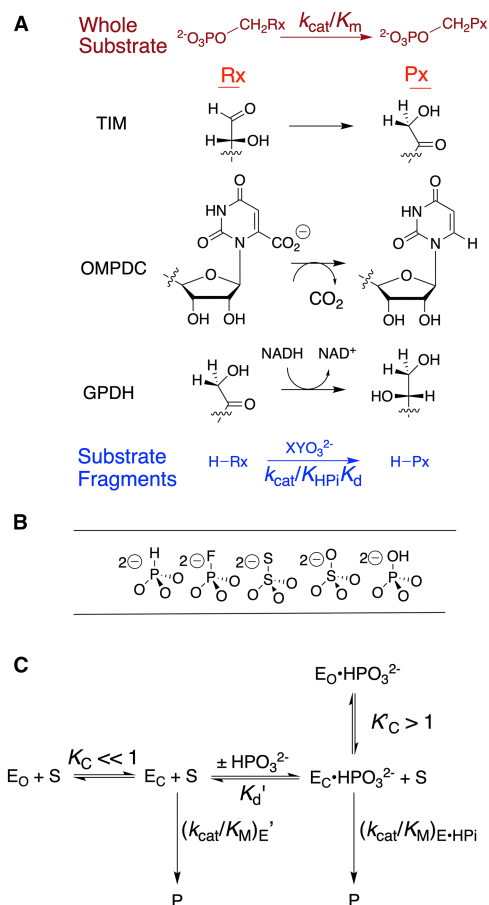
Figure 1. Enzyme-catalyzed reactions of whole substrates and substrate fragments.

(**A**) Proton transfer, decarboxylation and hydride transfer reactions of whole substrates $RCH_2OPO_3^{2-}$ (k_{cat}/K_m) and the substrate fragments $RH + HPO_3^{2-}$ ($k_{cat}/K_{HPi}K_d$) catalyzed by TIM, OMPDC, and GPDH, respectively. 'Rx' and 'Px' denote reactant and product states, respectively. The phosphoryl group of each whole substrate provides a total 11–13 kcal·mol^{-1} stabilization of the transition states for the catalyzed reaction, while 1.0 M phosphite dianion provides a 6–8 kcal·mol^{-1} stabilization of the transition states for the catalysis of each truncated substrate fragment [13]. (**B**) Dianion activators of the reactions of the substrate fragments [10]. (**C**) The model developed to rationalize activation of TIM, OMPDC and GPDH.

stabilization is that the phosphoryl group provides a strong anchor for attachment of the substrate to the enzyme. However, large effects from the binding of a charged group are observed in the absence of the anchoring covalent attachment between the substrate and its phosphoryl group, through the phosphite dianion activation of the reaction of truncated substrate fragments, as is also shown in Figure 1A. This activation corresponds to a 6–8 kcal·mol^{-1} stabilization of the transition state for the reaction of the respective truncated substrates by the neighboring phosphite dianion fragment, and a 4–6 kcal·mol^{-1} additional stabilization from the covalent attachment of the two substrate fragments [13,14]. The striking similarity in the relative kinetic parameters for the activation of TIM, OMPDC, and GPDH by HPO_3^{2-}, FPO_3^{2-}, $S_2O_3^{2-}$, SO_4^{2-}, and $HOPO_3^{2-}$ (Figure 1B) for reactions of their respective truncated substrates reveal a similarity in the specificity of these enzymes for dianion activation [10]. These results show that the binding pocket for the whole substrates can be usefully partitioned into a catalytic site, that carries out chemistry on the bound substrate, and a dianion activation site that utilizes protein-interactions to optimize catalysis at the catalytic site [10].

The ligand-gated conformational changes undergone by TIM, OMPDC, and GPDH each conform to the Koshland's induced fit model, where the binding energy of the dianion of the phosphoryl group (or phosphite dianion in the case of the binding of the substrate fragments) is utilized to induce an enzymatic conformational change, from the inactive open protein to the catalytically active closed form. These enzymes exist mainly in

the inactive open form, E_O, and the binding interactions between the substrate phosphoryl group and protein loops are utilized to stabilize the active closed form, E_C (Figure 1C) [12,13,15]. Enzyme activation results from the perturbation of the conformational equilibrium from $K_C \ll 1$ for the unliganded form of the enzyme, to $K_C \gg 1$ for the liganded enzyme (Figure 1C) [12,13,15]. The energetic barrier to conversion of E_O to E_C represents, minimally, the energetic cost for extrusion to bulk solvent of water molecules that solvate polar active site side chains at the open enzyme, and the entropic cost for the immobilization of large flexible protein loops and smaller catalytic amino acid side chains that accompanies conversion of E_O to E_C [13,15,16]. The nonreacting phosphoryl group (or substrate fragments such as phosphite dianion) play the role of 'cement' in Figure 1C to hold the protein catalyst in a rare stiff form, with high activity for catalysis of the reaction of the bound substrate, which is trapped in a structured protein cage.

Figure 1C shows a general mechanism by which enzymes utilize the binding interactions between the protein and nonreacting substrate fragments to obtain specificity in binding their transition states with a higher affinity than substrate [5,12]. This specificity is required for powerful enzyme catalysts, because the full expression of the large transition state binding energy at the Michaelis complex would result in effectively irreversible binding of substrate and/or product [5,12]. This specificity in transition state binding may be obtained either through the utilization of the intrinsic substrate binding energy to activate the substrate for enzymatic catalysis, by the introduction of destabilizing interactions into the substrate that are relieved at the enzymatic transition state, or, to directly activate the enzyme as shown in Figure 1C. The appeal of the model shown in Figure 1C is its potentially broad generalizability to any enzyme that conforms to Koshland's induced fit model.

The utilization of substrate binding energy to drive enzyme-activating conformational changes (Figure 1C) rationalizes results obtained from studies on an eclectic set of enzymatic reactions, which include the proton transfer reaction catalyzed by TIM [17,18], the decarboxylation reaction catalyzed by OMPDC [19], the hydride transfer reaction catalyzed by GPDH [20], the complex reaction catalyzed by 1-deoxy-D-xylulose-5-phosphate reductoisomerase [21,22], and more than 50-year-old results from studies on β-phosphoglucomutase [23]. In comparison, the results of experimental work over the past 25 years have not added greatly to the extensive body of evidence for the utilization of intrinsic substrate binding energy for substrate activation cited by Jencks in his 1975 review [5].

Finally, we note that the ligand-gated conformational changes of TIM, OMPDC, and GPDH each have the effect of optimizing the stabilizing interactions between the substrate phosphoryl group and a neighboring cationic side chain: K12 for TIM; R235 for OMPDC; and R269 for GPDH. The interactions between the protein side chain cations and substrate phosphoryl group provide 7.8, 5.6, and 9.1 kcal·mol^{-1} transition state stabilization for TIM [24], OMPDC [25], and GPDH [26], respectively. In each case, this is a significant fraction of the total 12 kcal·mol^{-1} transition state stabilization achieved through interactions with the phosphoryl group of the substrate. Each of these side chain cations sits on the protein surface and forms an ion pair with the buried phosphoryl group of the substrate [26]. The placement of these side chains at the protein surface favors efficient rescue of the catalytic activity that is lost when the side chain is truncated through mutation by small-molecule analogs of the truncated side chain [14,24–26].

Integration of experimental and computational studies

The empirical valence bond (EVB) approach [27] does an excellent job of modeling experimentally determined activation barriers for the conversion of enzyme-substrate Michaelis complexes to enzymatic transition states [28,29]. However, this approach focuses on modeling changes that occur during the actual chemical step of catalysis, and not on modeling the large-scale conformational changes upon substrate binding that can precede this step. Following from this, it is non-trivial to reliably model the free energy barrier for substrate binding that is coupled to extensive protein conformational changes, such as those observed for TIM, OMPDC, and GPDH. Despite this limitation, we have used the EVB approach with great success to rationalize the effects of ligand-gated conformational changes on the reactivity of substrates bound to TIM [30,31]. We hope to eventually generalize these calculations to model experimental results from studies on OMPDC, GPDH, and other enzymes that undergo ligand-driven conformational changes.

(1) Our proposal that the phosphite dianion-driven conformational change of TIM functions to activate this enzyme for deprotonation of enzyme-bound substrate predicts a role for the ligand-driven movement of amino acid side chains in substrate activation. We have performed EVB simulations [31], described below, to test predictions about the role of P166 [32–34], I170 [35–37], and L230 [35–38] in activation of the

caged complex between enzyme and substrate for deprotonation of the carbon-acid substrate by the side chain of E165 [39,40].

(2) We proposed that the dianionic phosphoryl group of the substrate DHAP serves the exclusive role of stabilizing an enzyme-substrate cage that shows high reactivity toward deprotonation of the bound carbon acid, and predicted that the substrate dianion serves as a spectator in this cage during deprotonation of the enzyme-bound substrate [16]. This prediction requires identical activation barriers for deprotonation of the Michaelis complex to the whole substrate DHAP, and to the substrate fragments glycolaldehyde (GA) and phosphite dianion [41,42], but it was not possible to saturate TIM with the substrate fragments. This prediction was, however, confirmed by the results of EVB calculations that are described below [30].

(3) The prime imperative for the observation of effective catalysis of deprotonation of weakly acidic α-carbonyl carbon of the substrates for TIM and other enzymes is to reduce the large thermodynamic barrier for formation of the carbanion reaction intermediate [18,43,44]. The results of EVB calculations to model the effect of site-directed substitutions on the thermodynamic barrier for TIM-catalyzed deprotonation of substrates DHAP and (*R*)-glyceraldehyde 3-phosphate (GAP) provide strong evidence that the precise placement of both polar and nonpolar side chains at the caged Michaelis complex serves to minimize the thermodynamic barrier to proton transfer to the enzyme.

Finally, we have performed extensive molecular dynamics simulations, using both conventional and enhanced sampling techniques, to analyze loop motion in apo and substrate-bound TIM. The results of these studies have been combined with EVB calculations to examine the effect of displacements of loop 6 from its closed form on catalytic activity. These studies represent one step toward the full computational modeling of substrate binding to TIM [45].

Early studies of loop dynamics and catalysis in triosephosphate isomerase

TIM catalyzes the reversible isomerization of DHAP to GAP in the eukaryotic glycolysis pathway [18,33,46,47]. This reaction proceeds through an enzyme-bound cis-enediolate intermediate. This enzyme is an ancient TIM-barrel enzyme that likely appeared early in evolution, and TIM-barrels are both ubiquitous and highly evolvable scaffolds [48–50]. As with most TIM-barrel proteins, TIM has several key active site loops (Figure 2) that decorate the scaffold and close over the active site upon interaction with the phosphoryl group of the substrate, thus creating a hydrophobic cage in which the TIM-catalyzed reaction can take place [16,30,51]. This desolvation of the active site is critical in order to elevate the pK_a of an active site glutamic acid — E165 using *y*TIM numbering — from 3.7 in aqueous solution to >6 in the TIM active site upon substrate binding [39,40,52], allowing E165 to deprotonate a substrate with a pK_a of ∼18 [53,54].

TIM is highly proficient, with k_{cat}/K_M values of $4.3 \times 10^5\,M^{-1}\,s^{-1}$ and $8.4 \times 10^6\,M^{-1}\,s^{-1}$ for the deprotonation of substrates DHAP and GAP, respectively [55]. It has been demonstrated that interactions between TIM and

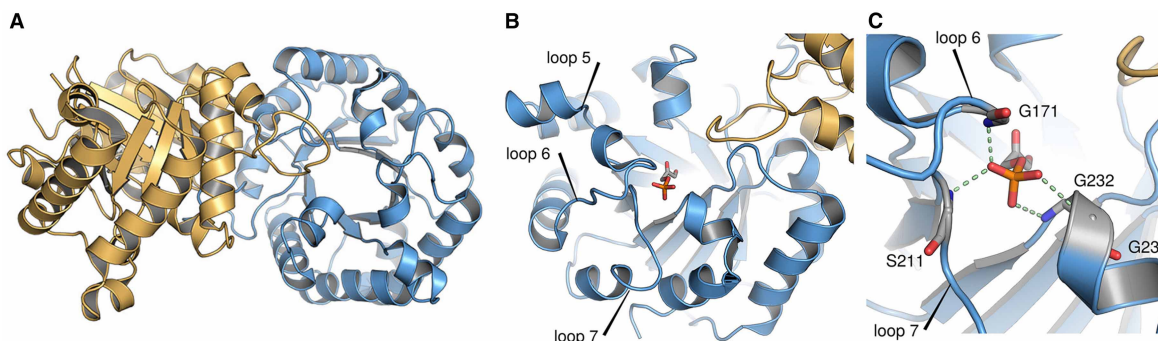**Figure 2. Snapshots of the structure of TIM.**
Overview of (**A**) the overall structure of yeast triosephosphate isomerase (*y*TIM; PDB ID: 1NEY [80,81]), showing also (**B**) key active site loops 5–7, as well as (**C**) a close up of the enzyme's active site. This figure is adapted from [45] (https://pubs.acs.org/doi/pdf/10.1021/jacs.8b09378), and is reproduced with permission from the American Chemical Society. Please note that requests for permissions regarding further reuse of this figure should be directed to the American Chemical Society.

the phosphoryl group of the substrate GAP can account for 80% of this enzyme's rate acceleration [53,56]. Tying in with this, there have been detailed studies of the activation of TIM for hydrolysis of the substrate fragment GA by phosphite dianion (HP$_i$), which have demonstrated that the binding of HP$_i$ to TIM results in a ~1000-fold increase in the second-order rate constant for the unactivated isomerization reaction of GA [(k_{cat}/K_M)$_E$ to (k_{cat}/K_M)$_{E\cdot HPi}$)] [8,57]. Therefore, the binding of phosphite to TIM results in a 4 kcal·mol^{-1} stabilization of the transition state for the unactivated reaction of GA [7]. It has been argued that a large fraction of the intrinsic binding energy of the phosphoryl group of the substrate (or the phosphite dianion) is used to drive the energetically demanding conformational change of the active site loops of TIM, from a catalytically unfavorable open conformation, to a catalytically competent closed conformation [7]. Notably, while the phosphate gripper loop, loop 6, undergoes a large conformational change (moving up to 7 Å as it closes over the active site), this change is coupled to more subtle but significant conformational changes in loop 7 [33]. This involves a 90° rotation of the G209–G210 peptide plane, which creates a steric clash with the P166 side chain, and which in turn triggers conformational movement along the E165–P166 plane that is critical for forcing E165 from a swung out position into the active site, in an optimal position for proton abstraction from the substrate. These motions are coupled to a substantial 180° rotation along the G210–S211 peptide bond. Therefore, while the conformational changes of loop 7 are more spatially confined than those of loop 6, they are no less critical to catalysis. Taken together, these features make TIM an ideal model system for studying the role of ligand-gated conformational changes in enzyme catalysis, while at the same time posing particular challenges for biomolecular simulations, as will be described in this contribution.

From a computational perspective, the movement of TIM loop 6 was one of the first functional enzyme motions to be investigated by means of molecule simulations [58]. In particular, Kollman [59], Karplus [60] and co-workers performed seminal molecular dynamics simulations *in vacuo*, using simple reaction co-ordinates, arguing that TIM loop closure is essentially a rigid-body type displacement. That is, they argued that the loop moves like a 'lid' that is attached to the protein by two hinges, the sequences of which are not conserved between different TIM-barrel proteins [61] (Figure 2). This early work has made TIM a classical system for understanding enzyme loop motion, and in fact the image of loop 6 motion as a two-state rigid-body motion is not only widespread [33,59,60,62–64], but also TIM has been used as an example of a proto-type for such motion in biological systems [65]. In parallel, there have been several studies of the mechanism (including cold-adaptation) of the TIM-catalyzed reaction (Figure 1A) using a range of computational approaches [30,31,45,66–70]. Curiously, however, despite extensive computational studies of TIM, and extensive experimental evidence for the role of ligand-gated conformational changes in catalysis by TIM and other enzymes [9–12,38], computational studies have generally failed to find an activating role for such changes, in part due to the short simulation timescales and/or simplified models involved.

Computational modeling of the role of ligand-gated conformational changes in catalysis by triosephosphate isomerase

To address the role of ligand-gated conformational changes in catalysis by TIM, as our starting point, we performed detailed EVB simulations of the mode of operation of a hydrophobic clamp (Figure 3A) in TIM [31], which acts to enhance the basicity of E165, thus facilitating efficient catalysis by this enzyme. Specifically, we considered both the TIM-catalyzed deprotonation of substrates DHAP and GAP by wild-type TIM, as well as by TIM variants with mutations of the residues forming this clamp (single and double I170A and L230A mutations, using *y*TIM numbering). Structural and biochemical characterization of these mutants in the TIM from *Trypanosoma brucei brucei* (*Tbb*TIM) [36,55] indicated diminished activity upon truncation of either side chain to alanine, while the structures of the different TIM variants in complex with the intermediate analog phospho-glycolate were nearly superimposable. The only significant difference between these structures was the presence of additional water molecules in the space made available by truncation of the hydrophobic side chains. Our EVB simulations of the different enzyme variants are able to reproduce the kinetic impact of these different mutations with excellent quantitative agreement with experiment (Figures 3B,C) [31], as well as allowing us (when combined with experimental analysis) to obtain a detailed overview of the breakdown of these changes into ground state and transition state effects. In particular, these calculations provide a linear free energy relationship (LFER), with a slope of 0.8, between the calculated activation barriers and Gibbs free energies for the TIM-catalyzed reactions studied in our work [31]. This combined experimental and computational analyses led us to conclude that
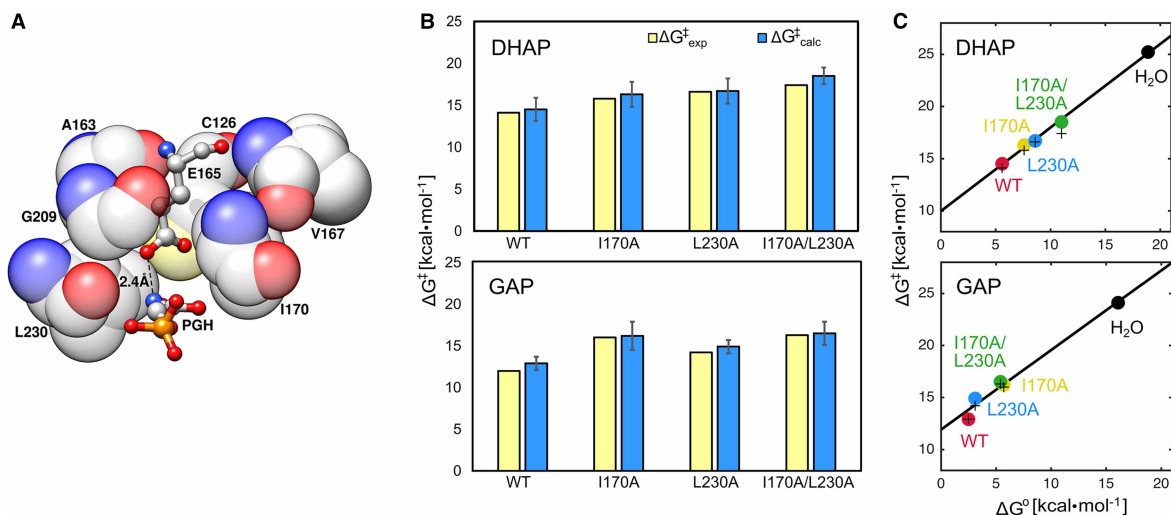
Figure 3. Modeling the Hydrophobic Clamp of TIM.

(A) An illustration of the hydrophobic clamp in TIM, formed by the hydrophobic side chains of residues I170 and L230 clamping the catalytic base E165. This figure is based on the active site of wild-type *Tbb*TIM (PDB ID: 1TRD [81,82]), in complex with the intermediate analog phosphoglycolhydroxamate (PGH). **(B)** A comparison of experimental ($\Delta G^{\ddagger}_{exp}$, yellow) and calculated ($\Delta G^{\ddagger}_{calc}$, blue) activation free energies for the deprotonation of (top) DHAP and (bottom) (R)-glyceraldehyde 3-phosphate (GAP) by wild-type and mutant TIMs. **(C)** The correlation between the experimental (+) and calculated (●) activation free energies ($\Delta G^{\ddagger}$), and the calculated reaction free energies (ΔG^{0}) for the deprotonation of (top) DHAP and (bottom) GAP by wild-type and mutant TIMs. Here, the correlation coefficients, calculated by linear regression analysis, are 0.9987 and 0.9921 for DHAP, and 0.9898 and 0.9909 for GAP (experimental and calculated values, respectively). All energies are presented in kcal·mol^{-1}. This figure is adapted from and based on data presented in ref. [31] (https://pubs.acs.org/doi/pdf/10.1021/jacs.7b05576), and is reproduced with permission from the American Chemical Society. Please note that requests for permissions regarding further reuse of this figure should be directed to the American Chemical Society.

the main role of these clamping side chains is to minimize the Gibbs free energy for substrate deprotonation, an effect that is largely expressed at the transition state for the TIM-catalyzed proton transfer reaction.

Following from this, we extended our EVB simulations of the full substrates DHAP and GAP [31] to also modeling the energetics for the deprotonation of the substrate fragments GA and GA·HP$_i$ [30] (Figure 4A). We note here that the kinetic parameters (k_{cat}/K_M, M^{-1}s^{-1}) for the TIM-catalyzed isomerization of the whole substrate GAP to form DHAP, as well as those for the corresponding phosphite dianion activation reactions of the substrate fragment GA, determined for 14 different wild-type and site-directed mutant forms of TIM, define an LFER with a slope of 1 between the activation barriers for the TIM-catalyzed reactions of the whole substrate and substrate fragments, by wild-type and mutant TIMs [41,42]. Similar relationships have been observed in other enzymes such as OMPDC [72] and GPDH [20], indicating that the primary role of the dianion activators is to stabilize the catalytically competent closed conformation of TIM (Figure 2). Our EVB simulations [30] of the deprotonation of the full substrate GAP as well as the substrate fragment GA and the fragments GA·HP$_i$ yield activation free energies ($\Delta G^{\ddagger}_{calc}$) of 12.9 ± 0.8 kcal·mol^{-1} for the full substrate GAP, and 15.0 ± 2.4 and 15.5 ± 3.5 kcal·mol^{-1} for the substrate fragments GA and GA·HP$_i$, respectively (Figure 4B). The increase in the activation barrier for the substrate fragments compared with the full substrate GAP is likely an entropic effect, due to the increased conformational space of the substrate fragments in the TIM active site, even in the presence of phosphite dianion (Figure 4C–H). However, the overall effect of the bound dianion on $\Delta G^{\ddagger}_{calc}$ is small at ≤ 2.6 kcal·mol^{-1}, compared with the much larger intrinsic binding energies of 12.8 and 5.8 kcal·mol^{-1} for the phosphoryl group of the substrate and the phosphite fragment that are utilized to stabilize the transition states for the TIM-catalyzed deprotonation of GAP and GA·HP$_i$, respectively [7,56]. This suggests that the dianion binding energy is fully expressed at the Michaelis complex, where it is utilized to drive an energetically unfavorable conformational change, and is the first computational evidence for the role of a ligand-gated conformational change in enzyme catalysis [30].
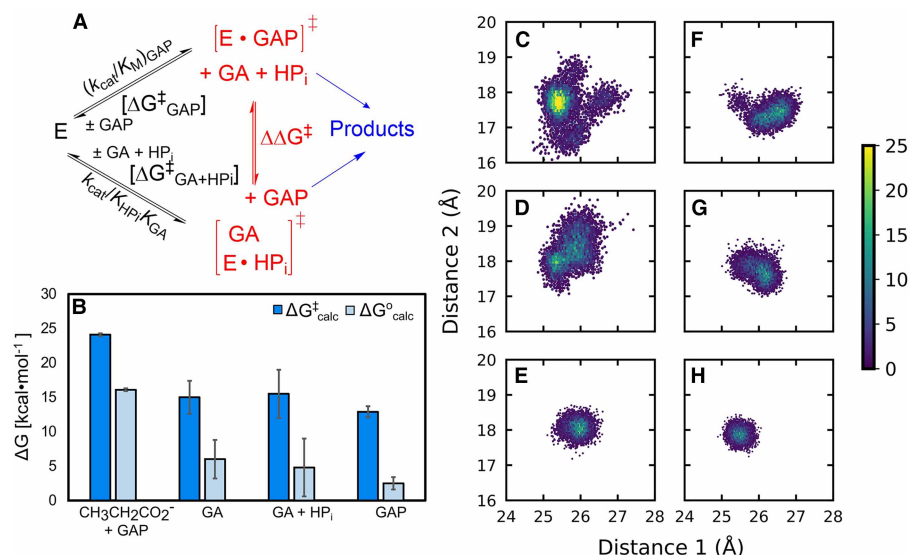
Figure 4. Modeling TIM-catalyzed reactions of the whole substrate and substrate fragments.

(**A**) Overview of the mechanisms for the TIM-catalyzed deprotonation of the full substrate GAP and the substrate fragments glycoaldehyde and phosphite dianion (GA·HP$_i$). (**B**) A comparison of calculated activation ($\Delta G^{\ddagger}_{calc}$, dark blue) and reaction (ΔG^{0}_{calc}, light blue) free energies for the non-enzymatic deprotonation of the full substrate GAP, as well as the corresponding TIM-catalyzed deprotonation of substrates glycoaldehyde (GA), GA·HP$_i$ and GAP. All energies are shown in kcal·mol^{-1}. (**C**) Population densities of the conformational space sampled by the substrate fragments (**C,F**) GA and (**D,G**) GA·HP$_i$, as well as (**E, H**) the full substrate GAP, at (**C–E**) the Michaelis complexes and (**F–H**) transition states for the TIM-catalyzed deprotonation of these substrates, obtained from EVB simulations, performed as described in ref. [30]. The data on the x- and y-axes based on distances between the donor carbon atoms of the relevant substrate and the backbone α-amino acid carbon atoms of D111 in Chain B and I19 in Chain A. For full details of the analysis see ref. [30]. This figure is adapted from and based on data presented in ref. [30] (https://pubs.acs.org/doi/10.1021/jacs.8b00251), and is reproduced with permission from the American Chemical Society. Please note that requests for permissions regarding further reuse of this figure should be directed to the American Chemical Society.

Finally, we have also been very interested in the motion of loop 6 itself. As described above, historically this loop motion has been described as a prototypical example of a two-state rigid-body motion [33,59,60,62–64]; however, these conclusions have in large part been based on short simulation timescales and/or simplified computational models. We recently performed detailed computational studies combining both microsecond conventional molecular dynamics simulations and enhanced sampling simulations of the conformational transitions of loop 6, using five crystal structure of the dimeric TIM from *Saccharomyces cerevisiae* (*y*TIM), coupled with EVB simulations [27,29] of the associated chemical step of catalysis [45]. We found that reliably modeling loop 6 motion is highly challenging and requires advanced sampling methods in order to be able to capture the closed conformation of the loop. These calculations demonstrated that contrary to being a rigid-body motion, loop 6 is in fact highly flexible, and samples multiple conformational states in the open conformation (Figure 5). However, the closed conformation was dominated by a single conformation of loops 6 and 7, that our simulations demonstrated to move in a concerted fashion in agreement with previous structural analysis [33]. However, despite sampling multiple open conformations, our EVB simulations [45] of the TIM-catalyzed deprotonation of DHAP at different conformations of loop 6 demonstrated that even slight displacements from the fully closed crystallographically observed loop conformation can be sufficient to abolish most of the catalytic activity of TIM; therefore, while the loop is overall flexible, full loop closure is required for efficient catalysis [16,45].

Finally, the importance of loop 6 flexibility to efficient catalysis can also be seen in mutational studies of rare variations of position 96 (proline in the wild-type) of the TIM from *Plasmodium falciparum* (*Pf*TIM) [73], which is analogous to the proline at position 168 in *Tbb*TIM [34]. In both cases, it is clear that this residue plays an important role in modulating the conformational transition of loop 6, and, most critically, in positioning E165 (*y*TIM numbering) in a catalytically competent position in the TIM active site (Figure 2).
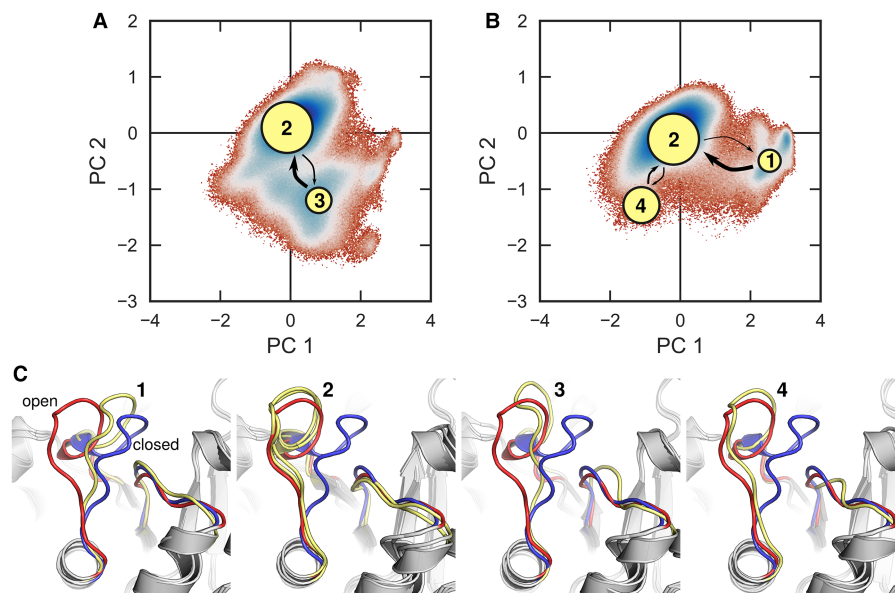
Figure 5. Modeling the open and closed conformations of TIM.

Markov state models (MSM) of (**A**) substrate-free TIM and (**B**) TIM in complex with substrate DHAP, superimposed on free energy surfaces defined in terms of the first two principal components, PC1 and PC2, obtained from conventional molecular dynamics simulations of each system (60 independent simulations, to a total of 22 μs of simulation time). The population of each node corresponding to a metastable state is represented through the area of the node, while the thickness of the arrows connecting the node corresponds to the transition probabilities, which are shown in the Supporting Information of ref. [45]. (**C**) A comparison of the crystal structures for TIM with open (red, PDB ID: 1YPI [71,81]) and closed (blue, PDB ID: 1NEY [80,81]) conformations of loop 6, as well as representative structures from the different centroids shown in panels (**A,B**). The numbering corresponds to the numbering of the different centroids. It can be seen here that the substrate-bound enzyme samples a semi-closed conformation (**1**), both systems sample an open conformation that is common to the two systems (**2**), while each samples a third open conformation that is unique to each system [(**3**) in the case of the substrate-free enzyme, (**4**) in the case of the substrate-bound enzyme]. For simulation details, see ref. [45]. This figure was originally presented in ref. [45] (https://pubs.acs.org/doi/pdf/10.1021/jacs.8b09378), and is reproduced with permission from the American Chemical Society. Please note that requests for permissions regarding further reuse of this figure should be directed to the American Chemical Society.

Loop motion and dimer assembly in triosephosphate isomerase

As shown in Figure 2, in the majority of cases, TIM is structurally a homodimer, and lends its name to the archetypal TIM-barrel fold comprising of eight α-helices and eight parallel β-sheets alternating along the protein backbone [45,48,49]. However, there do exist exceptions to this: in some organisms, TIM takes on instead a tetrameric form, and it has been argued that this change in oligomerization state can be functionally important [74–76]. In particular, the tetrameric form has been argued to provide more stability to the overall scaffold, allowing the enzyme to function at extremes of temperature [74,75]. Tying in with this, recent EVB studies comparing the temperature dependence of the TIM from the psychrophilic bacterium *Vibrius marinus* as well as yeast TIM indicated a shift in the enthalpy–entropy balance between the two enzymes, which was found to be due to greater mobility of key surface loops in the cold-adapted enzyme [70]. Therefore, scaffold rigidification through changes in oligomerization state could indeed plausibly allow the enzyme to withstand higher temperatures.

Principle component analysis on a range of TIM structures has shown that the TIM structure space can be divided into two groups: open and closed TIM structures, with a greater the distribution of structures in the open set than in the closed set [76]. This is supported by all-atom simulations of TIM loop motion which indicate that while TIM loop 6 is flexible and can take on multiple open conformations, the conformational space of the closed conformation of the loop is much more restricted [45]. In addition, elastic network modeling of monomeric, dimeric and tetrameric TIMs from different organisms demonstrated that oligomerization not only

PORTLAND PRESS

stabilized the structures, but also enhanced their functional loop motions (in particular of loops 6 and 7) [76]. Following from this, elastic network models have also shown that TIM-barrel proteins with conserved structure but without functional conservation can also have greatly different intrinsic dynamics tying in with their functional differences [77]. This is not a recent evolutionary event in TIM development, as studies of ancestral TIMs obtained through ancestral inference have indicated the presence of early evolutionary coupling between oligomerization and function [78]. Finally, mutagenesis studies of TIMs from the protozoan parasite *Trichomonas vagina* (*Tv*TIM) that are capable of dissociating into stable monomers, but that dimerize once substrate binds, have shown that the dimerization is necessary for assembly of a catalytically competent active site, but that as it is being assembled, the active site itself acts to stabilize the dimer [79]. Therefore, there is clear evidence for an interplay between global conformational changes, local loop motions, and TIM function, culminating in the critical importance of ligand-gated conformational changes to drive catalysis by these enzymes.

Concluding remarks

There is a tremendous wealth of biochemical and structural information that points to an important role for ligand-gated conformational changes in enzyme catalysis, in a wide range of enzymatic systems [13,21–23]. These studies demonstrate that ligand-gated conformational changes are one hallmark of the extraordinary efficiency of enzyme catalysis, compared with catalysis by small molecules in water. The binding energy of the phosphoryl group of the substrate that drives these conformational changes is utilized to mold enzymes into a high-energy catalytic form, and comparison of the structures of the open and closed forms of TIM has helped to identify the catalytic side chains that activate the TIM-bound substrate for a chemical reaction.

More recently, increases in computational power have allowed for both enzyme conformational changes and the fine details of the chemical mechanism to be studied in unprecedented detail. This contribution discusses examples of such computational studies, using TIM as a model system, that provide insight into the chemical step of catalysis by TIM [30,31], the role of loop conformational changes in driving the TIM-catalyzed reaction [45], and the role of oligomerization in allowing for TIMs to withstand extreme temperature conditions [76]. In particular, recent work on TIM loop motion [45] as well as the activation of the TIM-catalyzed deprotonation of the substrate fragment GA by phosphite dianion [30] show clear computational evidence for a role for the binding of anionic groups in driving a catalytically unfavorable conformational change. While our focus here has been on computational studies of a single enzyme, we have highlighted in this contribution the fact that analogs experimental data exists for a broad range of systems [9–13,15,16,20,72], and therefore we believe the conclusions from these computational studies can be extended to any enzyme that is activated by a ligand-gated conformational change. Finally, we demonstrate here how close synergy between theory and experiment is crucial for solving challenging questions with regard to our understanding of enzyme catalysis. This allows for even more challenging problems to be addressed, as described in the Outstanding Questions box.

Perspectives

- Enzymes are biological catalysts, which accelerate the rate of chemical reactions to levels necessary to support life. An understanding of their mechanism of action is critical to our understanding or all living systems.

- The experimental activation barrier to conversion of enzyme-substrate complexes to products have been successfully modeled using high-resolution protein crystal structures obtained by X-ray crystallographic analysis. The structures of unliganded enzymes in water often show flexible elements that undergo large conformational changes, which are driven by substrate binding to the protein. Several models have been developed to rationalize possible contributions of protein motions to enzymatic rate accelerations. A recent model emphasizes this role within the context of a general imperative for the coexistence of flexible structures for unliganded proteins and more rigid structures for their reactive Michaelis complexes.

- There is tremendous potential for experimental and theoretical studies to define mechanisms for enzyme action by characterizing the role of ligand-driven conformational change in activating enzymes for chemical catalysis.

Abbreviations

DHAP, dihydroxyacetone phosphate; EVB, empirical valence bond; GA, glycoaldehyde; GAP, (*R*)-glyceraldehyde 3-phosphate; GPDH, glycerol 3-phosphate dehydrogenase; HP$_i$, phosphite dianion; LFER, linear free energy relationship; MSM, Markov state models; OMPDC, orotidine 5′-monophosphate decarboxylase; PGH, phosphoglycolhydroxamate; TIM, triosephosphate isomerase.

Author Contributions

All authors contributed to the drafting of the manuscript and approved the final submission.

Funding

Competing Interests

The Authors declare that there are no competing interests associated with the manuscript.

References

1   Koshland, Jr, D.E. (1958) Application of a theory of enzyme specificity to protein synthesis. *Proc. Natl Acad. Sci. U.S.A.* **44**, 98–104 https://doi.org/10.1073/pnas.44.2.98
2   Blake, C.C.F., Koenig, D.F., Mair, G.A., North, A.C.T., Phillips, D.C. and Sarma, V.R. (1965) Structure of hen egg-white lysozyme: a three-dimensional Fourier synthesis at 2 Å resolution. *Nature* **206**, 757–761 https://doi.org/10.1038/206757a0
3   Alber, T., Banner, D.W., Bloomer, A.C., Petsko, G.A., Phillips, D., Rivers, P.S. et al. (1981) On the three-dimensional structure and catalytic mechanism of triose phosphate isomerase. *Philos. Trans. R. Soc. Lond. B.* **293**, 159–171 https://doi.org/10.1098/rstb.1981.0069
4   Koshland, D.E. (1993) The joys and vicissitudes of protein science. *Prot. Sci.* **2**, 1364–1368 https://doi.org/10.1002/pro.5560020821
5   Jencks, W.P. (1975) Binding energy, specificity, and enzymic catalysis: the circe effect. *Adv. Enzymol. Relat. Areas Mol. Biol.* **43**, 219–410 PMID: 892
6   Herschlag, D. (1988) The role of induced fit and conformational changes of enzymes in specificity and catalysis. *Bioorg. Chem.* **16**, 62–96 https://doi.org/10.1016/0045-2068(88)90038-7
7   Amyes, T.L. and Richard, J.P. (2007) Enzymatic catalysis of proton transfer at carbon: activation of triosephosphate isomerase by phosphite dianion. *Biochemistry* **46**, 5841–5854 https://doi.org/10.1021/bi700409b
8   Go, M.K., Amyes, T.L. and Richard, J.P. (2009) Hydron transfer catalyzed by triosephosphate isomerase. Products of the direct and phosphite-activated isomerization of [1-^{13}C]-glycolaldehyde in D$_2$O. *Biochemistry* **48**, 5769–5778 https://doi.org/10.1021/bi900636c
9   Amyes, T.L., Richard, J.P. and Tait, J.J. (2005) Activation of orotidine 5′-monophosphate decarboxylase by phosphite dianion: the whole substrate is the sum of two parts. *J. Am. Chem. Soc.* **127**, 15708–15709 https://doi.org/10.1021/ja055493s
10   Reyes, A.C., Zhai, X., Morgan, K.T., Reinhardt, C.J., Amyes, T.L. and Richard, J.P. (2015) The activating oxydianion binding domain for enzyme-catalyzed proton transfer, hydride transfer and decarboxylation: specificity and enzyme architecture. *J. Am. Chem. Soc.* **137**, 1372–1382 https://doi.org/10.1021/ja5123842
11   Tsang, W.-Y., Amyes, T.L. and Richard, J.P. (2008) A substrate in pieces: allosteric activation of glycerol 3-phosphate dehydrogenase (NAD$^+$) by phosphite dianion. *Biochemistry* **47**, 4575–4582 https://doi.org/10.1021/bi8001743
12   Richard, J.P. (2019) Protein flexibility and stiffness enable efficient enzymatic catalysis. *J. Am. Chem. Soc.* **141**, 3320–3331 https://doi.org/10.1021/jacs.8b10836
13   Amyes, T.L. and Richard, J.P. (2013) Specificity in transition state binding: the Pauling model revisited. *Biochemistry* **52**, 2021–2035 https://doi.org/10.1021/bi301491r
14   Reyes, A.C., Amyes, T.L. and Richard, J.P. (2016) Enzyme architecture: self-assembly of enzyme and substrate pieces of glycerol-3-phosphate dehydrogenase into a robust catalyst of hydride transfer. *J. Am. Chem. Soc* **138**, 15251–15259 https://doi.org/10.1021/jacs.6b09936
15   Amyes, T.L., Malabanan, M.M., Zhai, X., Reyes, A.C. and Richard, J.P. (2017) Enzyme activation through the utilization of intrinsic dianion binding energy. *Protein Eng. Des. Sel.* **30**, 159–168 https://doi.org/10.1093/protein/gzw064
16   Richard, J.P., Amyes, T.L., Goryanova, B. and Zhai, X. (2014) Enzyme architecture: on the importance of being in a protein cage. *Curr. Opin. Chem. Biol.* **21**, 1–10 https://doi.org/10.1016/j.cbpa.2014.03.001
17   Richard, J.P., Zhai, X. and Malabanan, M.M. (2014) Reflections on the catalytic power of a TIM-barrel. *Bioorg. Chem.* **57**, 206–212 https://doi.org/10.1016/j.bioorg.2014.07.001
18   Richard, J.P. (2012) A paradigm for enzyme-catalyzed proton transfer at carbon: triosephosphate isomerase. *Biochemistry* **51**, 2652–2661 https://doi.org/10.1021/bi300195b
19   Richard, J.P., Amyes, T.L. and Reyes, A.C. (2018) Orotidine 5′-monophosphate decarboxylase: probing the limits of the possible for enzyme catalysis. *Acc. Chem. Res.* **51**, 960–969 https://doi.org/10.1021/acs.accounts.8b00059
20   He, R., Reyes, A.C., Amyes, T.L. and Richard, J.P. (2018) Enzyme architecture: the role of a flexible loop in activation of glycerol-3-phosphate dehydrogenase for catalysis of hydride transfer. *Biochemistry* **57**, 3227–3236 https://doi.org/10.1021/acs.biochem.7b01282
21   Kholodar, S.A., Allen, C.L., Gulick, A.M. and Murkin, A.S. (2015) The role of phosphate in a multistep enzymatic reaction: reactions of the substrate and intermediate in pieces. *J. Am. Chem. Soc.* **137**, 2748–2756 https://doi.org/10.1021/ja512911f

22 Kholodar, S.A. and Murkin, A.S. (2013) DXP reductoisomerase: reaction of the substrate in pieces reveals a catalytic role for the nonreacting phosphodianion group. *Biochemistry* **52**, 2302–2308 https://doi.org/10.1021/bi400092n

23 Ray,, W.J., Long, J.W. and Owens, J.D. (1976) An analysis of the substrate-induced rate effect in the phosphoglucomutase system. *Biochemistry* **15**, 4006–4017 https://doi.org/10.1021/bi00663a015

24 Go, M.K., Amyes, T.L. and Richard, J.P. (2010) Rescue of K12G mutant TIM by NH_4^+ and alkylammonium cations: the reaction of an enzyme in pieces. *J. Am. Chem. Soc.* **132**, 13525–13532 https://doi.org/10.1021/ja106104h

25 Barnett, S.A., Amyes, T.L., Wood, M.B., Gerlt, J.A. and Richard, J.P. (2010) Activation of R235A mutant orotidine 5′-monophosphate decarboxylase by the guanidinium cation: effective molarity of the cationic side chain of Arg-235. *Biochemistry* **49**, 824–826 https://doi.org/10.1021/bi902174q

26 Reyes, A.C., Koudelka, A.P., Amyes, T.L. and Richard, J.P. (2015) Enzyme architecture: optimization of transition state stabilization from a cation–phosphodianion pair. *J. Am. Chem. Soc.* **137**, 5312–5315 https://doi.org/10.1021/jacs.5b02202

27 Warshel, A. and Weiss, R.M. (1980) An empirical valence bond approach for comparing reactions in solutions and in enzymes. *J. Am. Chem. Soc.* **102**, 6218–6226 https://doi.org/10.1021/ja00540a008

28 Shurki, A., Derat, E., Barrozo, A. and Kamerlin, S.C.L. (2015) How valence bond theory can help you understand your (bio)chemical reaction. *Chem. Soc. Rev.* **44**, 1037–1052 https://doi.org/10.1039/C4CS00241E

29 Kamerlin, S.C.L. and Warshel, A. (2011) The empirical valence bond model: theory and applications. *Wiley Interdiscip. Rev. Comput. Mol. Sci.* **1**, 30–45 https://doi.org/10.1002/wcms.10

30 Kulkarni, Y.S., Liao, Q., Byléhn, F., Amyes, T.L., Richard, J.P. and Kamerlin, S.C.L. (2018) The role of ligand-driven conformational changes in enzyme catalysis: modeling the reactivity of the catalytic cage of triosephosphate isomerase. *J. Am. Chem. Soc.* **140**, 3854–3857 https://doi.org/10.1021/jacs.8b00251

31 Kulkarni, Y.S., Liao, Q., Petrović, D., Krüger, D.M., Strodel, B., Amyes, T.L. et al. (2017) Enzyme architecture: modeling the operation of a hydrophobic clamp in catalysis by triosephosphate isomerase. *J. Am. Chem. Soc.* **139**, 10514–10525 https://doi.org/10.1021/jacs.7b05576

32 Zhai, X., Amyes, T.L., Wierenga, R.K., Loria, J.P. and Richard, J.P. (2013) Structural mutations that probe the interactions between the catalytic and dianion activation sites of triosephosphate isomerase. *Biochemistry* **52**, 5928–5940 https://doi.org/10.1021/bi401019h

33 Wierenga, R.K. ., Kapetaniou, E. G. and Venkatesan, R. (2010) Triosephosphate isomerase: a highly evolved biocatalyst. *Cell. Mol. Life Sci.* **67**, 3961–3982 https://doi.org/10.1007/s00018-010-0473-9

34 Casteleijn, M.G., Alahuhta, M., Groebel, K., El-Sayed, I., Augustyns, K., Lambeir, A.-M. et al. (2006) Functional role of the conserved active site proline of triosephosphate isomerase. *Biochemistry* **45**, 15483–15494 https://doi.org/10.1021/bi061683j

35 Kursula, I. and Wierenga, R.K. (2003) Crystal structure of triosephosphate isomerase complexed with 2-phosphoglycolate at 0.83-Å resolution. *J. Biol. Chem.* **278**, 9544–9551 https://doi.org/10.1074/jbc.M211389200

36 Richard, J.P., Amyes, T.L., Malabanan, M.M., Zhai, X., Kim, K.J., Reinhardt, C.J. et al. (2016) Structure–function studies of hydrophobic residues that clamp a basic glutamate side chain during catalysis by triosephosphate isomerase. *Biochemistry* **55**, 3036–3047 https://doi.org/10.1021/acs.biochem.6b00311

37 Malabanan, M.M., Koudelka, A.P., Amyes, T.L. and Richard, J.P. (2012) Mechanism for activation of triosephosphate isomerase by phosphite dianion: the role of a hydrophobic clamp. *J. Am. Chem. Soc.* **134**, 10286–10298 https://doi.org/10.1021/ja303695u

38 Malabanan, M.M., Amyes, T.L. and Richard, J.P. (2011) Mechanism for activation of triosephosphate isomerase by phosphite dianion: the role of a ligand-driven conformational change. *J. Am. Chem. Soc.* **133**, 16428–16431 https://doi.org/10.1021/ja208019p

39 Zhai, X., Reinhardt, C.J., Malabanan, M.M., Amyes, T.L. and Richard, J.P. (2018) Enzyme architecture: amino acid side-chains that function to optimize the basicity of the active site glutamate of triosephosphate isomerase. *J. Am. Chem. Soc.* **140**, 8277–8286 https://doi.org/10.1021/jacs.8b04367

40 Malabanan, M.M., Nitsch-Velasquez, L., Amyes, T.L. and Richard, J.P. (2013) Magnitude and origin of the enhanced basicity of the catalytic glutamate of triosephosphate isomerase. *J. Am. Chem. Soc.* **135**, 5978–5981 https://doi.org/10.1021/ja401504w

41 Zhai, X., Amyes, T.L. and Richard, J.P. (2015) Role of loop-clamping side chains in catalysis by triosephosphate isomerase. *J. Am. Chem. Soc.* **137**, 15185–15197 https://doi.org/10.1021/jacs.5b09328

42 Zhai, X., Amyes, T.L. and Richard, J.P. (2014) Enzyme architecture: remarkably similar transition states for triosephosphate isomerase-catalyzed reactions of the whole substrate and the substrate in pieces. *J. Am. Chem. Soc.* **136**, 4145–4148 https://doi.org/10.1021/ja501103b

43 Gerlt, J.A. and Gassman, P.G. (1993) An explanation for rapid enzyme-catalyzed proton abstraction from carbon acids: importance of late transition states in concerted mechanisms. *J. Am. Chem. Soc.* **115**, 11552–11568 https://doi.org/10.1021/ja00077a062

44 Amyes, T.L. and Richard, J.P. (1996) Determination of the pK_a of ethyl acetate: brønsted correlation for deprotonation of a simple oxygen ester in aqueous solution. *J. Am. Chem. Soc.* **118**, 3129–3141 https://doi.org/10.1021/ja953664v

45 Liao, Q., Kulkarni, Y., Sengupta, U., Petrović, D., Mulholland, A.J., van der Kamp, M.W. et al. (2018) Loop motion in triosephosphate isomerase is not a simple open and shut case. *J. Am. Chem. Soc.* **140**, 15889–15903 https://doi.org/10.1021/jacs.8b09378

46 Knowles, J.R. (1991) Enzyme catalysis: not different, just better. *Nature* **350**, 121–124 https://doi.org/10.1038/350121a0

47 Knowles, J.R. and Albery, W.J. (1977) Perfection in enzyme catalysis: the energetics of triosephosphate isomerase. *Acc. Chem. Res.* **10**, 105–111 https://doi.org/10.1021/ar50112a001

48 Wierenga, R.K. (2001) The TIM-barrel fold: a versatile framework for efficient enzymes. *FEBS Lett.* **492**, 193–198 https://doi.org/10.1016/S0014-5793(01)02236-0

49 Nagano, N., Orengo, C.A. and Thornton, J.M. (2002) One fold with many functions: the evolutionary relationships between TIM barrel families based on their sequences, structures and functions. *J. Mol. Biol.* **321**, 741–765 https://doi.org/10.1016/S0022-2836(02)00649-6

50 Sterner, R. and Höcker, B. (2005) Catalytic versatility, stability, and evolution of the $(\beta/\alpha)_8$-barrel enzyme fold. *Chem. Rev.* **105**, 4038–4055 https://doi.org/10.1021/cr030191z

51 Malabanan, M.M., Amyes, T.L. and Richard, J.P. (2010) A role for flexible loops in enzyme catalysis. *Curr. Opin. Struct. Biol.* **20**, 702–710 https://doi.org/10.1016/j.sbi.2010.09.005

52 Deng, H., Dyer, R.B. and Callender, R. (2019) Active-site Glu165 activation in triosephosphate isomerase and its deprotonation kinetics. *J. Phys. Chem. B* **123**, 4230–4241 https://doi.org/10.1021/acs.jpcb.9b02981

53 Richard, J.P. (1984) Acid-base catalysis of the elimination and isomerization reactions of triose phosphates. *J. Am. Chem. Soc.* **106**, 4926–4936 https://doi.org/10.1021/ja00329a050

54 Richard, J.P. and Amyes, T.L. (2001) Proton transfer at carbon. *Curr. Opin. Chem. Biol.* **5**, 626–633 https://doi.org/10.1016/S1367-5931(01)00258-7

55 Malabanan, M.M., Go, M.K., Amyes, T.L. and Richard, J.P. (2011) Wildtype and engineered monomeric triosephosphate isomerase from *Trypanosoma brucei*: partitioning of reaction intermediates in D$_2$O and activation by phosphite dianion. *Biochemistry* **50**, 5767–5779 https://doi.org/10.1021/bi2005416

56 Amyes, T.L., O'Donoghue, A.C. and Richard, J.P. (2001) Contribution of phosphate intrinsic binding energy to the enzymatic rate acceleration for triosephosphate isomerase. *J. Am. Chem. Soc.* **123**, 11325–11326 https://doi.org/10.1021/ja016754a

57 Amyes, T.L. and Richard, J.P. (2007) Proton transfer to and from carbon in model reactions. In *Hydrogen Transfer Reactions* (Hynes, J.T., Klinman, J.P., Limbach, H.-H. and Schowen, R.L., eds), pp. 949–973, Wiley-VCH Verlag GmbH & Co., Weinheim, Germany

58 Alagona, G., Desmeules, P., Ghio, C. and Kollman, P.A. (1984) Quantum mechanical and molecular mechanical studies on a model for the dihydroxyacetone phosphate-glyceraldehyde phosphate isomerization catalyzed by triose phosphate isomerase (TIM). *J. Am. Chem. Soc.* **106**, 3623–3632 https://doi.org/10.1021/ja00324a035

59 Brown, F.K. and Kollman, P.A. (1987) Molecular dynamics simulations of "loop closing" in the enzyme triose phosphate isomerase. *J. Mol. Biol.* **198**, 533–546 https://doi.org/10.1016/0022-2836(87)90298-1

60 Joseph, D., Petsko, G. and Karplus, M. (1990) Anatomy of a conformational change: hinged "lid" motion of the triosephosphate isomerase loop. *Science* **249**, 1425–1428 https://doi.org/10.1126/science.2402636

61 Xiang, J., Sun, J. and Sampson, N.S. (2001) The importance of hinge sequence for loop function and catalytic activity in the reaction catalyzed by triosephosphate isomerase. *J. Mol. Biol.* **307**, 1103–1112 https://doi.org/10.1006/jmbi.2001.4536

62 Williams, J.C. and McDermott, A.E. (1995) Dynamics of the flexible loop of triose-phosphate isomerase: the loop motion is not ligand gated. *Biochemistry* **34**, 8309–8319 https://doi.org/10.1021/bi00026a012

63 Rozovsky, S., Jogl, G., Tong, L. and McDermott, A.E. (2001) Solution-state NMR investigations of triosephosphate isomerase active site loop motion: ligand release in relation to active site loop dynamics. *J. Mol. Biol.* **310**, 271–280 https://doi.org/10.1006/jmbi.2001.4673

64 Kempf, J.G., Jung, J.-Y., Ragain, C., Sampson, N.S. and Loria, J.P. (2007) Dynamic requirements for a functional protein hinge. *J. Mol. Biol.* **368**, 131–149 https://doi.org/10.1016/j.jmb.2007.01.074

65 Papaleo, E., Saladino, G., Lambrughi, M., Lindorff-Larsen, K., Gervasio, F.L. and Nussinov, L. (2016) The role of protein loops and linkers in conformational dynamics and allostery. *Chem. Rev.* **116**, 6391–6423 https://doi.org/10.1021/acs.chemrev.5b00623

66 Bash, P.A., Field, M.J., Davenport, R.C., Petsko, G.A., Ringe, D. and Karplus, M. (1991) Computer simulation and analysis of the reaction pathway of triosephosphate isomerase. *Biochemistry* **30**, 5826–5832 https://doi.org/10.1021/bi00238a003

67 Åqvist, J. and Fothergill, M. (1996) Computer simulation of the triosephosphate isomerase catalyzed reaction. *J. Biol. Chem.* **271**, 10010–10016 https://doi.org/10.1074/jbc.271.17.10010

68 Cui, Q. and Karplus, M. (2001) Triosephosphate isomerase: a theoretical comparison of alternative pathways. *J. Am. Chem. Soc.* **123**, 2284–2290 https://doi.org/10.1021/ja002886c

69 Cui, Q. and Karplus, M. (2002) Quantum mechanics/molecular mechanics studies of triosephosphate isomerase-catalyzed reactions: effect of geometry and tunneling on proton-transfer rate constants. *J. Am. Chem. Soc.* **124**, 3093–3124 https://doi.org/10.1021/ja0118439

70 Åqvist, J. (2017) Cold adaptation of triosephosphate isomerase. *Biochemistry* **56**, 4169–4176 https://doi.org/10.1021/acs.biochem.7b00523

71 Lolis, E., Albert, T., Davenport, R.C., Rose, D., Hartman, F.C. and Petsko, G.A. (1990) Structure of yeast triosephosphate isomerase at 1.9 Å resolution. *Biochemistry* **29**, 6609–6618 https://doi.org/10.1021/bi00480a009

72 Goldman, L.M., Amyes, T.L., Goryanova, B., Gerlt, J.A. and Richard, J.P. (2014) Enzyme architecture: deconstruction of the enzyme-activating phosphodianion interactions of orotidine 5′-monophosphate decarboxylase. *J. Am. Chem. Soc.* **136**, 10156–10165 https://doi.org/10.1021/ja505037v

73 Pareek, V., Samanta, M., Joshi, N.V., Balaram, H., Murthy, M.R.N. and Balaram, P. (2016) Connecting active-site loop conformations and catalysis in triosephosphate isomerase: insights from a rare variation at residue 96 in the plasmodial enzyme. *ChemBioChem* **17**, 620–629 https://doi.org/10.1002/cbic.201500532

74 Walden, H., Bell, G.S., Russell, R.J.M., Siebers, B., Hensel, R. and Taylor, G.L. (2001) Tiny TIM: a small, tetrameric, hyperthermostable triosephosphate isomerase. *J. Mol. Biol.* **306**, 745–757 https://doi.org/10.1006/jmbi.2000.4433

75 Walden, H., Taylor, G.L., Lorentzen, E., Pohl, E., Lilie, H., Schramm, A. et al. (2004) Structure and function of a regulated archaeal triosephosphate isomerase adapted to high temperature. *J. Mol. Biol.* **342**, 861–875 https://doi.org/10.1016/j.jmb.2004.07.067

76 Katebi, A.R. and Jernigan, R.L. (2014) The critical role of the loops of triosephosphate isomerase for its oligomerization, dynamics, and functionality. *Protein Sci.* **23**, 213–228 https://doi.org/10.1002/pro.2407

77 Tiwari, S.P. and Reuter, N. (2016) Similarity in shape dictates signature intrinsic dynamics despite no functional conservation in TIM barrel enzymes. *PLoS Comput. Biol.* **12**, e1004834–e1004834 https://doi.org/10.1371/journal.pcbi.1004834

78 Schulte-Sasse, M., Pardo-Ávila, F., Pulido-Mayoral, N.O., Vázquez-Lobo, A., Costas, M., García-Hernández, E. et al. (2019) Structural, thermodynamic and catalytic characterization of an ancestral triosephosphate isomerase reveal early evolutionary coupling between monomer association and function. *FEBS J.* **286**, 882–900 https://doi.org/10.1111/febs.14741

79 Jimenez-Sandoval, P., Vique-Sanchez, J.L., Hidalgo, M.L., Velazquez-Juarez, G., Diaz-Quezada, C., Arroyo-Navarro, L.F. et al. (2017) A competent catalytic active site is necessary for substrate induced dimer assembly in triosephosphate isomerase. *Biochim. Biophys. Acta Proteins Proteom.* **1865**, 1423–1432 https://doi.org/10.1016/j.bbapap.2017.07.014

80 Jogl, G., Rozovsky, S., McDermott, A.E. and Tong, L. (2003) Optimal alignment for enzymatic proton transfer: structure of the michaelis complex of triosephosphate isomerase at 1.2-Å resolution. *Proc. Natl. Acad. Sci. U.S.A.* **100**, 50–55 https://doi.org/10.1073/pnas.0233793100

81 Berman, H.M., Westbrook, J., Feng, Z., Gilliland, G., Bhat, T.N., Weissig, H. et al. (2000) The protein data bank. *Nucleic Acids Res.* **28**, 235–242 https://doi.org/10.1093/nar/28.1.235

82 Noble, M.E., Zeelen, J.P. and Wierenga, R.K. (1993) Structures of the "open" and "closed" state of trypanosomal triosephosphate isomerase, as observed in a new crystal form: implications for the reaction mechanism. *Proteins* **16**, 311–326 https://doi.org/10.1002/prot.340160402